

# Unsupervised Domain Adaptation via Deep Hierarchical Optimal Transport

Yingxue Xu<sup>1,2</sup>, Guihua Wen<sup>1</sup>, Yang Hu<sup>3</sup>, Pei Yang<sup>1,\*</sup>

<sup>1</sup> South China University of Technology, <sup>2</sup> The Hong Kong University of Science and Technology, <sup>3</sup> University of Oxford  
yxueb@connect.ust.hk, crghwen@scut.edu.cn, yang.hu@ndm.ox.ac.uk, yangpei@scut.edu.cn

## Abstract

Unsupervised domain adaptation is a challenging task that aims to estimate a transferable model for unlabeled target domain by exploiting source labeled data. Optimal Transport (OT) based methods recently have been proven to be a promising direction for domain adaptation due to their competitive performance. However, most of these methods coarsely aligned source and target distributions, leading to the over-aligned problem where the category-discriminative information is mixed up although domain-invariant representations can be learned. In this paper, we propose a Deep Hierarchical Optimal Transport method (DeepHOT) for unsupervised domain adaptation. The main idea is to use hierarchical optimal transport to learn both domain-invariant and category-discriminative representations by mining the rich structural correlations among domain data. The DeepHOT framework consists of a domain-level OT and an image-level OT, where the latter is used as the ground distance metric for the former. The image-level OT captures structural associations of local image regions that are beneficial to image classification, while the domain-level OT learns domain-invariant representations by leveraging the underlying geometry of domains. However, due to the high computational complexity, the optimal transport based models are limited in some scenarios. To this end, we propose a robust and efficient implementation of the DeepHOT framework by approximating origin OT with sliced Wasserstein distance in image-level OT and using a mini-batch unbalanced optimal transport for domain-level OT. Extensive experiments show that DeepHOT surpasses the state-of-the-art methods in four benchmark datasets. Code will be released on GitHub.

## Introduction

In the context of traditional machine learning, one generally assumes that the training and test data should be independent and identically distributed. However, in many practical vision problem, various factors, such as different acquisition conditions, changing lighting conditions, presence of background, can break this assumption and cause discrepancies in data distribution (a.k.a. domain shift). Domain adaptation methods aim to mitigate this issue by finding a shared representation between domains where a classifier can be learned and used for target domain (Courty et al. 2017b). In this work, we

focus on unsupervised domain adaptation (UDA), where no label is available in the target domain.

Fruitful works (Tzeng et al. 2014; Long et al. 2015; Yan et al. 2017; Ganin et al. 2016; Sun and Saenko 2016) have been done for unsupervised domain adaptation, where the core idea boils down to align distributions across domains. Among others, optimal transport based methods have shown superiority in various unsupervised domain adaptation tasks by leveraging the underlying geometry of domains (Courty et al. 2017b,a). Optimal transport applies ground metric to measure the distance between pairwise samples from source and target domains, so that the discrepancy of domains can be measured by minimizing matching cost point-by-point. However, most of these methods coarsely aligned source and target distributions, and suffered from the over-aligned issue. That is to say, although domain-invariant representation is learned by domain alignment, the discriminative information for each category would be mixed up.

In this work, we propose a Deep Hierarchical Optimal Transport framework (DeepHOT) for unsupervised domain adaptation. It aims to learn domain-invariant yet category-discriminative representations by mining the structural correlations in both domain-level and image-level. The DeepHOT framework comprises a domain-level OT and an image-level OT. The image-level OT computes the optimal transport distance for image pair, which is used as the ground distance metric for the domain-level OT to estimate the optimal transport distance between domains. In the vision problem, local features of image are considered to provide discriminative and transferable information across categories. Optimal transport has recently provided a solution to encode correspondences between local regions of two images for enhancing discriminative features, and its efficacy has been proved in few-shot learning (Zhang et al. 2020). Therefore, by representing an image as a set of local regions, we use the image-level OT to measure point-to-point distance across samples. The image-to-image distance obtained by image-level OT is used as the ground distance metric for the domain-level OT to measure the distance between domains, which are represented as the sets of samples. In this way, not only domains can be aligned by domain-level OT, but discriminative power of samples are also enhanced by image-level OT. Therefore, DeepHOT is able to learn domain-invariant yet category-discriminative representations, even though no labeled data can be accessed

\*Corresponding author

in target domain.

However, despite the performance superiority, optimal transport based methods have the drawback of high computational complexity. To this end, we propose a robust and efficient implementation of the DeepHOT framework. The key approaches to address this issue are three-fold. First, for image-level OT, sliced Wasserstein distance (SWD) (Lee et al. 2019a) is applied to compute the discrepancy between pairwise images, which has been proved to be more efficient than Earth mover distance in time complexity. Second, for domain-level OT, we compute the domain distance over mini-batches and use the averaged result as a proxy for the original problem. And then, time complexity would be considerably reduced if using a small mini-batch. Third, it is difficult for mini-batch OT methods to converge to the true transport plan when the batch size decreases. Therefore, we exploit mini-batch unbalanced optimal transport (UOT) (Fratras et al. 2021) for domain-level OT, which can provide a more robust solution to the mini-batch sampling.

The contributions of this work are summarized as follows: (1) We propose a novel deep hierarchical optimal transport method for unsupervised domain adaptation to learn domain-invariant yet category-discriminative representations. To the best of our knowledge, it is the first deep hierarchical optimal transport method for UDA. (2) We propose a robust and efficient implementation of the DeepHOT framework. (3) Extensive experiments on four benchmark domain adaptation datasets show significant improvement over state-of-the-art methods.

## Related Work

### Unsupervised Domain Adaptation

Unsupervised domain adaptation aims to learn a model on the labeled source domain that can adapt the target domain in which labels are unavailable. Most existing works can be broadly classified into two categories: discrepancy-based domain alignment and adversarial learning.

**Discrepancy-based domain alignment.** This kind of methods (Tzeng et al. 2014; Yan et al. 2017) tend to explicitly minimize a divergence that measures the gap between the source and target domains. A typical discrepancy metric, Maximum Mean Discrepancy (MMD) (Tzeng et al. 2014), has been extensively applied to domain adaptation tasks and (Gretton et al. 2012) further proposed multi-kernels MMD. Moreover, Weighted-MMD (WDAN) (Yan et al. 2017) integrated class prior with original MMD by class-specific auxiliary weights. Another measure that can be utilized for domain alignment is covariance, leading to a method Deep Correlation Alignment (Deep CORAL) (Sun and Saenko 2016). These methods only consider aligning the marginal distribution, and however, Deep Transfer Network (DTN) (Zhang et al. 2015) proposed a conditional alignment method using pseudo labels of target domain. (Wang et al. 2020) learned a joint distribution by dynamically quantifying the relative importance of marginal and class-conditional distribution. Another branch is based on optimal transport which is illustrated in next subsection.

**Adversarial learning.** Another critical type of methods

rely on adversarial training, where the core idea is to maximally confuse domain classifier so as to learn domain-invariant representation. Based on this idea, Domain Adversarial Neural Network (DANN) adversarially (Ganin et al. 2016) learned a feature extractor and a domain discriminator, and (Tzeng et al. 2017) had the similar solution for UDA by simply fooling a GAN’s discriminator. In addition, there are some adversarial image generation methods (Liu, Breuel, and Kautz 2017; Sankaranarayanan et al. 2018) that impose a class-conditioning or cycle consistency constraint to capture discriminative embeddings.

Note that our method DeepHOT belongs to one of discrepancy-based domain alignment methods that minimize the matching cost by optimal transportation to align source and target domains.

### Optimal Transport for Domain Adaptation

Optimal Transport (OT) theory has been theoretically proven to be competitive in the context of domain adaptation (Redko, Habrard, and Sebban 2017), and (Courty et al. 2017b) first introduced OT into unsupervised domain adaptation. Then OT-reglab (Courty, Flamary, and Tuia 2014) and JDOT (Courty et al. 2017a) further took label information into account where they assumed joint feature/label distribution of source and target domains could be estimated by a non-linear transformation. DEEPJDOT (Damodaran et al. 2018) extended JDOT into a deep learning-based version, and JUMBOT (Fratras et al. 2021) alleviated the sampling effect of mini-batch optimal transport which allowed optimal transport for large-scale datasets in an end-to-end way. Recently, TIDOT (Nguyen et al. 2021) has jointly mitigated both data shift and label shift by teacher-student framework with optimal transport, and LAMDA (Le et al. 2021) has explicitly defined the label shift and minimized it by optimal transportation on the latent space. The main difference between the proposed DeepHOT method and the related work is that DeepHOT is a generalized hierarchical optimal transport formulation consisting of domain-level OT and image-level OT for domain adaptation, while the related work such as JUMBOT (Fratras et al. 2021) involve domain-level OT only.

Another member of optimal transport family is hierarchical optimal transport that is a generalization of OT. It has been recently applied to different tasks such as multi-modal distribution alignment (Lee et al. 2019b), document representation (Yurochkin et al. 2019), semi-supervised learning (Taherkhani et al. 2020) and multi-view learning (Luo, Xu, and Carin 2020). To date, only one work HOT-DA (Hamri et al. 2021) has used hierarchical optimal transport for UDA that leveraging clustering structure between domains. However, they suffer from a main limitation that their approach can be only applied to small-size datasets. Different from this, to the best of our knowledge, we propose the first deep learning-based HOT model that can be trained over mini-batch in an end-to-end way, which allows hierarchical optimal transport to be applied for large-scale datasets.

## The Proposed DeepHOT Method

### Overview

Let  $\mathbf{X}_s = \{\mathbf{x}_i^s\}_{i=1}^{N_s}$  be a set of data drawn from a distribution  $\mu_s$  on the source domain, associated with a set of class labels  $\mathbf{Y}_s = \{\mathbf{y}_i^s\}_{i=1}^{N_s}$ , and  $\mathbf{X}_t = \{\mathbf{x}_i^t\}_{i=1}^{N_t}$  a data set drawn from a distribution  $\mu_t$  on the target domain. The labels for the target domain are not available during training.

In the unsupervised DA problem, Optimal Transport allows to bring source and target distributions closer by finding optimal transport plan between pairwise samples from source and target domains. Formally, OT is commonly defined by the Kantorovich formulation (Kantorovich 2006) to search a probabilistic coupling  $\gamma \in \Pi(\mu_s, \mu_t)$  between the distribution  $\mu_s$  of source domain and  $\mu_t$  of target domain:

$$\mathcal{W}_d(\mu_s, \mu_t, c) = \inf_{\gamma \in \Pi(\mu_s, \mu_t)} \int_{\Omega_s \times \Omega_t} c(\mathbf{x}^s, \mathbf{x}^t) d\gamma(\mathbf{x}^s, \mathbf{x}^t) \quad (1)$$

where  $c(\cdot)$  is the ground metric that measures the discrepancy between pairwise samples  $\mathbf{x}^s$  and  $\mathbf{x}^t$ . Here,  $\Omega_s$  (resp.  $\Omega_t$ ) is a compact input measurable space related to source (resp. target) domain, and  $\Pi(\mu_s, \mu_t)$  can be understood as the joint probability measure with marginals  $\mu_s$  and  $\mu_t$ .

Here we use discrete optimal transport theory to formulate both domain-level and image-level distances. The empirical distribution  $\mu_s$  for source domain is formulated as  $\mu_s = \sum_{i=1}^{N_s} p_i^s \delta_{\mathbf{x}_i^s}$  where  $\delta_{\mathbf{x}_i^s}$  is the Dirac function located at  $\mathbf{x}_i^s$ , and  $p_i^s$  is probability mass associated with  $\mathbf{x}_i^s$  and belongs to the probability simplex, i.e.  $\sum_{i=1}^{N_s} p_i^s = 1$ . The empirical distribution  $\mu_t$  for target domain can be formulated in the similar way. In this case, we can adapt Kantorovich OT formulation (Kantorovich 2006) to the discrete case.

In a discrete setting, optimal transport between the empirical distributions is formulated as:

$$\mathcal{W}_d(\mu_s, \mu_t, c) = \min_{\gamma \in \mathcal{B}} \langle \gamma, \mathbf{C} \rangle_F \quad (2)$$

where  $\mathcal{B} = \{\gamma \in (\mathbb{R}^+)^{N_s \times N_t} | \gamma \mathbf{1}_{N_t} = \mu_s, \gamma^T \mathbf{1}_{N_s} = \mu_t\}$ , and  $\mathbf{1}_d$  is a  $d$ -dimensional vector of ones. In this case,  $\mathcal{B}$  refers to the set of probabilistic couplings between the two empirical distributions.  $\langle \cdot \rangle_F$  is the Frobenius dot product and  $\mathbf{C} \geq 0$  is the cost matrix, whose term  $C(i, j) = c(\mathbf{x}_i^s, \mathbf{x}_j^t)$  represents the dissimilarity between pairwise samples from source and target domains. In the general case, this cost function  $c(\cdot)$  is chosen as Euclidean or cosine distance.

As previously mentioned, local features of image can help to enhance discriminative power when aligning the marginal distribution across domains. Here, when decomposing an image into a set of local regions, we can use optimal transport  $\mathcal{W}_{img}$  to measure the distance between samples instead of Euclidean distance, which can be used as the cost function  $c(\cdot)$  of problem (2). As such, the problem (2) becomes a nested OT formulation, i.e. a general Hierarchical Optimal Transport (HOT) formulation:

$$\mathcal{H}(\mu_s, \mu_t) = \mathcal{W}_d(\mu_s, \mu_t, \mathcal{W}_{img}) \quad (3)$$

where correspondences are resolved at two levels: the outer level resolves domain-correspondences while the inner level

resolves point-wise correspondences between pairwise samples from source and target domains. Our key insight is depicted in Figure 1, where image-level OT permits to encode correlations between local image regions to enhance discriminative power for domain alignment that is achieved by domain-level OT.

Note that domain-level (outer level) OT and image-level (inner level) OT can be any optimal transport algorithm (Chizat et al. 2018; Frogner et al. 2015; Lee et al. 2019a; Liero, Mielke, and Savaré 2018). Next we will propose a robust and efficient solution for the generalized DeepHOT framework. In the remainder, we detail the OT formulation for both domain-level (outer level) and image-level (inner level). Finally optimization process and computational complexity of HOT formulation are presented.

### Domain-Level OT

The domain-level OT aims to learn the optimal mappings between the samples from source and target domains. To reduce computational complexity, the domain-level OT is trained over mini-batch using deep learning in an end-to-end way. The averaged result among mini-batches is used as a proxy for the original problem.

To build mini-batch, we select  $n$  samples from  $\mathbf{X}_s$  and  $\mathbf{X}_t$ . Then optimal transport over mini-batch becomes

$$\mathcal{W}_d^n(\mu_s^n, \mu_t^n, \mathcal{W}_{img}) = \min_{\gamma^n \in \mathcal{B}^n} \langle \gamma^n, \mathbf{C}^n \rangle_F \quad (4)$$

where  $\mathbf{C}^n$  is a square matrix of size  $n$  and  $\mathcal{B}^n = \{\gamma \in (\mathbb{R}^+)^{n \times n} | \gamma \mathbf{1}_n = \mu_s^n, \gamma^T \mathbf{1}_n = \mu_t^n\}$ . The term of cost matrix  $\mathbf{C}^n$  can be computed by optimal transport on image-level  $\mathcal{W}_{img}$ , which will be illustrated in next subsection.

In practice, however, it was proven that the solution to optimal transport over mini-batch tends to be less sparse, and causes undesired pairings between samples that shouldn't have been matched in true OT (Fratras et al. 2021). A variant (Fratras et al. 2021) of Unbalanced Optimal Transport (UOT) recently has been theoretically validated to deal with this issue by relaxing marginal constraints. Therefore, we propose to use unbalanced mini-batch optimal transport for the domain-level OT to alleviate the side effect of mini-batch sampling. Then the problem (4) becomes

$$\mathcal{W}_d^n(\mu_s^n, \mu_t^n, \mathcal{W}_{img}) = \min_{\gamma^n \in \mathcal{B}^n} \langle \gamma^n, \mathbf{C}^n \rangle_F + \varepsilon KL(\gamma^n | \mu_s^n \otimes \mu_t^n) + \tau (D_\phi(\gamma_s^n || \mu_s^n) + D_\phi(\gamma_t^n || \mu_t^n)) \quad (5)$$

where  $\gamma^n$  is the transport plan over mini-batch,  $\gamma_s^n$  and  $\gamma_t^n$  are plan's marginals. Here,  $D_\phi$  is Csiszàr divergences,  $\tau$  is the marginal penalization and  $\varepsilon \geq 0$  is the regularization coefficient. KL is the Kullback-Leibler divergence.

This OT formulation (5) is used to replace  $\mathcal{W}_d$  in Eq. (3), which naturally proposes a deep learning-based version of HOT method  $\mathcal{H}^n(\cdot)$ , i.e. Deep **H**ierarchical **O**ptimal **T**ransport (DeepHOT):

$$\mathcal{H}^n(\mu_s^n, \mu_t^n) = \mathcal{W}_d^n(\mu_s^n, \mu_t^n, \mathcal{W}_{img}) \quad (6)$$

### Image-Level OT

The image-level OT aims to align the image pairs by capturing the correlations among the local regions of images. To

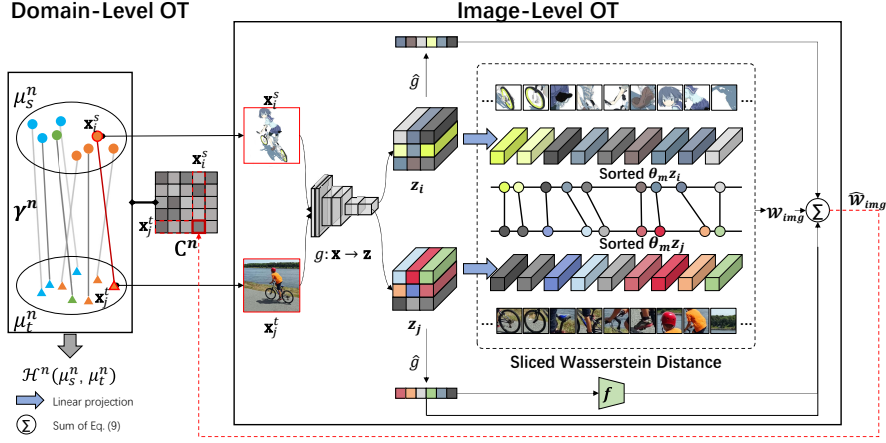


Figure 1: Overview architecture of DeepHOT. It consists of domain-level OT and an image-level OT, where the output of latter is used as the term of cost matrix  $\mathbf{C}^n$  for the former. And then the distance  $\mathcal{H}^n(\mu_s^n, \mu_t^n)$  between  $\mu_s^n$  and  $\mu_t^n$  domains can be computed via domain-level OT. Color in domain-level OT refers to class.

approximate OT in a deep learning-based manner, we first formulate an embedding function (e.g. CNN)  $g: \mathbf{x} \rightarrow \mathbf{z}$  that maps the input into the latent space  $\mathbf{Z}$ , and the classifier  $f: \mathbf{z} \rightarrow \mathbf{y}$  which maps the latent space into the label space  $\mathbf{Y}$ .

Here latent space can be modelled by any feature layer. In the unsupervised DA task, optimal transport on image-level aims to utilize local information to learn discriminative features. As such, we use the last convolution layer of a CNN to interpret this latent space that preserves the structural information of feature maps  $\mathbf{z} \in \mathbb{R}^{H \times W \times C}$  ( $H$  and  $W$  denote the spatial size of feature maps and  $C$  refers to the channel dimension). And then  $\mathbf{z}$  is viewed as a collection of feature vectors  $[\mathbf{z}^1, \mathbf{z}^2, \dots, \mathbf{z}^{HW}]$  where each element  $\mathbf{z}^k \in \mathbb{R}^{C \times 1}$  ( $1 \leq k \leq HW$ ) is a vector. The strength of viewing the feature map as a collection of local feature vectors is that it allows us to use the optimal transport to mine the structural relationships among local regions of two images, in order to learn the discriminative and transferable information across categories.

In this case, an image  $\mathbf{x}_i$  can be represented with a collection of local feature vectors  $[\mathbf{z}_i^1, \mathbf{z}_i^2, \dots, \mathbf{z}_i^{HW}]$ . Optimal transport can be used to capture the local correspondences between two images which are important for classification. Then we can formulate optimal transport on image-level as

$$\begin{aligned} \mathcal{W}_{img}(\mathbf{x}_i^s, \mathbf{x}_j^t, c) &= \min_{\gamma^{img} \in \Pi(g(\mathbf{x}_i^s), g(\mathbf{x}_j^t))} \langle \gamma^{img}, \mathbf{C}^{img} \rangle \\ &= \min_{\gamma^{img} \in \Pi(\mathbf{z}_i, \mathbf{z}_j)} \sum_u \sum_v \gamma_{uv}^{img} c(\mathbf{z}_i^u, \mathbf{z}_j^v) \end{aligned} \quad (7)$$

where  $c(\mathbf{z}_i^u, \mathbf{z}_j^v) = \|\mathbf{z}_i^u - \mathbf{z}_j^v\|^2$ . However, problem (7) can be solved by linear programming, which is not efficient, especially when combining with domain-level OT. And thus we introduce a learnable Sliced Wasserstein Distance (Lee et al. 2019a; Luo, Xu, and Carin 2020) (SWD) to approximate

problem (7) for an more efficient OT formulation:

$$\begin{aligned} \mathcal{W}_{img}(\mathbf{x}_i^s, \mathbf{x}_j^t, c) &= \frac{1}{M} \sum_{m=1}^M c(\text{sort}(\theta_m^\top g(\mathbf{x}_i^s)), \text{sort}(\theta_m^\top g(\mathbf{x}_j^t))) \\ &= \frac{1}{M} \sum_{m=1}^M \|\text{sort}(\theta_m^\top \mathbf{z}_i) - \text{sort}(\theta_m^\top \mathbf{z}_j)\|^2 \end{aligned} \quad (8)$$

where  $\{\theta_m\}_{m=1}^M$  contains  $M$  linear projectors  $\theta_m \in \mathbb{R}^{C \times 1}$  that allow to solve one-dimensional OT problems. In this manner, we simplify a linear programming problem (7) into equation (8) with the help of a sorting algorithm, where the sorting function sorts the elements of the vector in ascending order, such that  $\forall 0 \leq k \leq HW - 1, (\theta_m^\top \mathbf{z}_i)^{(k)} \leq (\theta_m^\top \mathbf{z}_i)^{(k+1)}$ . Then we calculate the Euclidean distance between the sorted vectors and get the averaged result across projectors.

The above term (SWD) together with Euclidean distance are jointly applied as cost function of domain-level OT (i.e. Problem (5)) to align marginal distribution. Furthermore, following (Courtney et al. 2017a; Damodaran et al. 2018; Fatras et al. 2021), we also use the semantic constraint to handle a conditional distribution shift. Finally, the cost function of domain-level OT is re-formulated as

$$\begin{aligned} \widehat{\mathcal{W}}_{img}((\mathbf{x}_i^s, \mathbf{y}_i^s), \mathbf{x}_j^t, c) &= \eta_1 \frac{1}{M} \sum_{m=1}^M \|\text{sort}(\theta_m^\top g(\mathbf{x}_i^s)) - \text{sort}(\theta_m^\top g(\mathbf{x}_j^t))\|^2 \\ &\quad + \eta_2 \|\hat{g}(\mathbf{z}_i) - \hat{g}(\mathbf{z}_j)\|^2 + \eta_3 \mathcal{L}_{ce}(\mathbf{y}_i^s, f(\hat{g}(\mathbf{x}_j^t))) \end{aligned} \quad (9)$$

where  $\hat{g}(\cdot)$  refers to global average pooling of  $g(\cdot)$  and  $\eta_1, \eta_2, \eta_3$  are the parameters controlling the tradeoff between these terms. In this way, the term of cost matrix in problem (5) has  $C(i, j) = \widehat{\mathcal{W}}_{img}((\mathbf{x}_i^s, \mathbf{y}_i^s), \mathbf{x}_j^t, c)$ , and DeepHOT model (6) can be interpreted as

$$\mathcal{H}^n(\mu_s^n, \mu_t^n) = \mathcal{W}_d^n(\mu_s^n, \mu_t^n, \widehat{\mathcal{W}}_{img}) \quad (10)$$

Following the common setting, to avoid *catastrophic forgetting* (Shmelkov, Schmid, and Alahari 2017) that refers to

---

**Algorithm 1** The DeepHOT Algorithm

---

**Input:** Source data as  $\mathbf{X}_s = \{\mathbf{x}_i^s\}_{i=1}^{N_s}$ , target data as  $\mathbf{X}_t = \{\mathbf{x}_i^t\}_{i=1}^{N_t}$ .  $T$  is set as the number of training iterations, and  $n$  refers to the batch-size for training.

**Output:** The optimal parameters of embedding function  $g$  and classifier  $f$ ;

- 1: Randomly initialize  $\{\theta_m\}_{m=1}^M$  of  $M$  projections.
- 2: **for**  $t = 1$  to  $T$  **do**
- 3:   Sample mini-batch from source data  $\{(\mathbf{x}_i^s, \mathbf{y}_i^s)\}_{i=1}^n$  and target data  $\{\mathbf{x}_i^t\}_{i=1}^n$ .
- 4:   Fix  $g$ ,  $f$  and  $\{\theta_m\}_{m=1}^M$ .
- 5:   **for**  $(\mathbf{x}_i^s, \mathbf{y}_i^s), \mathbf{x}_j^t$  **do**
- 6:     Calculate  $\widehat{\mathcal{W}}_{img}((\mathbf{x}_i^s, \mathbf{y}_i^s), \mathbf{x}_j^t, c)$  according to Eq. (9).  
    // Image-level OT
- 7:      $C(i, j) \leftarrow \widehat{\mathcal{W}}_{img}((\mathbf{x}_i^s, \mathbf{y}_i^s), \mathbf{x}_j^t, c)$
- 8:   **end for**
- 9:    $\mathbf{C}^n = \{C(i, j)\}_{i,j}^{n,n}$
- 10:   Optimize  $\gamma^n$  via Sinkhorn-Knopp matrix scaling algorithm (Chizat et al. 2018; Frogner et al. 2015); // Domain-level OT
- 11:    $\gamma^n \leftarrow \arg \min_{\gamma^n \in \mathcal{B}^n} \mathcal{W}_d^n(\mathbf{x}_s^n, \mathbf{x}_t^n, \widehat{\mathcal{W}}_{img})$  // Eq. (5)
- 12:   Fix  $\gamma^n$  and calculate the loss of DeepHOT  $\mathcal{H}^n(\mathbf{x}_s^n, \mathbf{x}_t^n)$  following Eq. (10) and (5).
- 13:   Calculate the total loss function  $\mathcal{L}^n$  according to Eq. (11).
- 14:   Update  $g$ ,  $f$  and  $\{\theta_m\}_{m=1}^M$  by SGD (Sutskever et al. 2013).
- 15: **end for**

---

a degradation in the source domain, the final loss function  $\mathcal{L}$  of DeepHOT over mini-batch is integrated with the cross entropy term  $\mathcal{L}_{ce}$  on the source data:

$$\mathcal{L}^n = \mathcal{L}_{ce}(\mathbf{X}_s^n, \mathbf{Y}_s^n) + \mathcal{H}^n(\mu_s^n, \mu_t^n) \quad (11)$$

### Optimization and Computational Complexity

We propose an efficient learning algorithm to solve the HOT problem (10) for UDA, which is a new member of Hierarchical Optimal Transport family, combining deep learning-based Unbalanced Optimal Transport on domain-level with Slice Wasserstein Distance on image-level. The details of optimization procedure are presented in Alg. 1.

In general, OT formulation on each level of HOT model implemented by Wasserstein Distance (or Earth Mover Distance) is solved by linear programming algorithms where the computational complexity is  $\mathcal{O}(N^3 \log(N))$  and  $N = \max(N_s, N_t)$  on domain-level, as well as  $\mathcal{O}(K^3 \log(K))$  and  $K = HW$  on image-level.

Compared with the above regular setting, our DeepHOT implementation has great advantages on computational complexity: (1) The complexity of domain-level OT over mini-batch solved by the generalized Sinkhorn-Knopp matrix scaling algorithm (Chizat et al. 2018; Frogner et al. 2015) is  $\mathcal{O}(n^2)$  in which  $n \ll N$  is the size of mini-batch. It allows to apply HOT model for large scale datasets. For the whole dataset, complexity is  $\mathcal{O}(\frac{N}{n} \times n^2) = \mathcal{O}(N \times n)$  which is far smaller than  $\mathcal{O}(N^3 \log(N))$ . (2) On image-level, the complexity of calculating the transport map is  $\mathcal{O}(K \log(K))$ , where  $K$  is small as the spatial size of feature maps (e.g.  $K = HW$ ) down-sampled by CNN is limited. The complexity of calculating  $M$  projections of a  $d$ -dimensional

probability density functions is  $\mathcal{O}(MN^d)$  which dominates the primary complexity. Hence the overall computational complexity of image-level OT formulation is  $\mathcal{O}(MN^d)$ . In this case, we can trade off the computational complexity of image-level formulation by setting the number  $M$  of projections.

## Experiments

In this section, we evaluate our method on four benchmark datasets for UDA tasks, and investigate the efficacy of each component in Ablation Study. Training efficiency is also evaluated and we intuitively validate the effectiveness of proposed method by visualization technique. We rely on the POT package (Flamary and Courty 2017) and PyTorch tools for all experimental implementation.

### Datasets

**Office-Home** (Venkateswara et al. 2017) contains 15,500 images from four domains: Artistic images (A), ClipArt (C), Product images (P) and Real-World (R), consisting of 65 categories for each domain. We evaluate our method over all 12 adaptation tasks and report results on the test target datasets. **Digits** involves three challenging UDA scenarios following the evaluation protocol of (Fratras et al. 2021): USPS (Hull 1994) to MNIST (LeCun et al. 1998) (U→M), MNIST to M-MNIST (Ganin et al. 2016) (M→MM) and SVHN (Netzer et al. 2011) to MNIST (S→M). It includes four domains: MNIST with 60,000 images, USPS with 7,291 images, SVHN with 73,212 images and M-MNIST that is colored version of MNIST with 10 classes of digits. **Office-31** (Saenko et al. 2010) consists of 4652 images from 31 categories, collected from three domains including Amazon (2817 images), Webcam (795 images) and DSLR (498 images), respectively, where every pair UDA task is evaluated as in (Huang et al. 2022). **VisDA** (Peng et al. 2017) is a large-scale dataset for UDA including two domains: Synthetic and Real-World. It contains 152,397 synthetic images and 55,388 real-world images that share 12 classes. Following the setting of (Fratras et al. 2021), we train all methods on Synthetic and test on VisDA validation set.

### Results

We compare our method against state-of-the-art methods: DANN (Ganin et al. 2016), CDAN-E (Long et al. 2018), DEEPJDOT (Damodaran et al. 2018), ALDA (Chen et al. 2020), ROT (Balaji, Chellappa, and Feizi 2020), ADDA (Tzeng et al. 2017), DWL (Xiao and Zhang 2021), CaCo (Huang et al. 2022) and JUMBOT (Fratras et al. 2021), which are all based on deep learning with RESNET50 (He et al. 2016) pretrained on ImageNet for all datasets except digits. The settings on digits are presented in supplementary materials. All these settings of experimental pipeline follow the public implementations of JUMBOT (Fratras et al. 2021) that is the closest to our method for fair comparisons. We present Accuracy score (in %) reported in JUMBOT or their own papers unless otherwise stated. We conduct each experiment three times and report the average results and error bars. The error bars for the comparison

Table 1: Results on Office-Home (RESNET50).

Method	A-C	A-P	A-R	C-A	C-P	C-R	P-A	P-C	P-R	R-A	R-C	R-P	avg
RESNET50	34.9	50.0	58.0	37.4	41.9	46.2	38.5	31.2	60.4	53.9	41.2	59.9	46.1
DANN	46.2	65.2	73.0	54.0	61.0	65.2	52.0	43.6	72.0	64.7	52.3	79.2	60.7
CDAN-E	52.8	71.4	76.1	59.7	70.6	71.5	59.8	50.8	77.7	71.4	58.1	83.5	67.0
DEEPIJDOT	53.4	71.7	77.2	62.8	70.2	71.4	60.2	50.2	77.1	67.7	56.5	80.7	66.6
ALDA	53.7	70.1	76.4	60.2	72.6	71.5	56.8	51.9	77.1	70.2	56.3	82.1	66.6
ROT	47.2	70.8	77.6	61.3	69.9	72.0	55.4	41.4	77.6	69.9	50.4	81.5	64.6
JUMBOT	55.3	75.5	80.8	65.5	74.4	74.9	<b>65.4</b>	52.7	79.3	<b>74.2</b>	59.9	83.4	70.1
<b>DeepHOT (ours)</b>	<b>57.0</b> $\pm 0.2$	<b>77.3</b> $\pm 0.3$	<b>81.9</b> $\pm 0.2$	<b>66.5</b> $\pm 0.1$	<b>77.4</b> $\pm 0.5$	<b>78.0</b> $\pm 0.6$	63.8 $\pm 0.5$	<b>54.8</b> $\pm 0.3$	<b>81.5</b> $\pm 0.2$	73.4 $\pm 0.4$	<b>60.0</b> $\pm 0.3$	<b>84.5</b> $\pm 0.3$	<b>71.3</b>

Table 2: Results on Office-31 (RESNET50).

Method	A→W	D→W	W→D	A→D	D→A	W→A	Avg
RESNET50	68.4	96.7	99.3	68.9	62.5	60.7	76.1
DANN	82.0	96.9	99.1	79.7	68.2	67.4	82.2
ADDA	86.2	96.2	98.4	77.8	69.5	68.9	82.9
DWL	89.2	99.2	<b>100.0</b>	91.2	73.1	69.8	87.1
CaCo	89.7	98.4	<b>100.0</b>	91.7	73.1	72.8	87.6
DEEPIJDOT	88.9	98.5	99.6	88.2	72.1	70.1	86.2
JUMBOT	93.0 $\pm 0.4$	98.7 $\pm 0.2$	<b>100.0<math>\pm 0</math></b>	<b>93.0<math>\pm 0.3</math></b>	73.6 $\pm 0.3$	<b>75.3<math>\pm 0.2</math></b>	88.9
<b>DeepHOT(ours)</b>	<b>95.7<math>\pm 0.5</math></b>	<b>99.3<math>\pm 0.2</math></b>	<b>100.0<math>\pm 0</math></b>	92.8 $\pm 0.4$	<b>74.2<math>\pm 0.3</math></b>	75.1 $\pm 0.3$	<b>89.5</b>

Table 3: Results on Digits.

Method	U→M	M→MM	S→M	Avg
DANN	92.2 $\pm 0.3$	96.1 $\pm 0.6$	88.7 $\pm 1.2$	92.3
CDAN-E	<b>99.2<math>\pm 0.1</math></b>	95.0 $\pm 3.4$	90.9 $\pm 4.8$	95.0
ALDA	97.0 $\pm 1.4$	96.4 $\pm 0.3$	96.1 $\pm 0.1$	96.5
DEEPIJDOT	96.4 $\pm 0.3$	91.8 $\pm 0.2$	95.4 $\pm 0.1$	94.5
JUMBOT	98.2 $\pm 0.1$	97.0 $\pm 0.3$	98.9 $\pm 0.1$	98.0
<b>DeepHOT (ours)</b>	99.0 $\pm 0.2$	<b>97.6<math>\pm 0.3</math></b>	<b>99.1<math>\pm 0.1</math></b>	<b>98.6</b>

Table 4: Results on VisDA (RESNET50).

Method	Accuracy
CDAN-E	70.1
ALDA	70.5
DEEPIJDOT	68.0
ROBUST OT	66.3
JUMBOT	72.5
<b>DeepHOT (ours)</b>	<b>73.5<math>\pm 0.5</math></b>

methods are also shown if they are available in their papers. Details about experimental setup are provided in supplementary materials.

Note that we don’t compare DeepHOT with HOT-DA (Hamri et al. 2021). The reason is that HOT-DA can be only evaluated in the subset of large-scale datasets mentioned above as it suffers from high computational complexity. Furthermore, HOT-DA doesn’t claim details of sampling subsets and code is unavailable.

**Results on Office-Home.** As shown in Table 1, our DeepHOT achieves the best accuracy on average with a margin of 1.2% compared with JUMBOT, which confirms the superiority of our approach over the other methods, benefiting from discriminative power improvement of image-level OT. Note that on 10 of 12 UDA scenarios the proposed DeepHOT performs best, where the highest performance gain arises in C→R with 3.1%. In most cases, DeepHOT keeps consistent improvement: for example, it achieves 1%-3% improvement among 9 UDA tasks, and thus the results are reliable.

**Results on Office-31.** Note that results of JUMBOT are reproduced using its official code as they don’t report them on their paper. As we can see from Table 2, our approach gets the best accuracy on 4 of 6 UDA tasks although the

averaged gain is only 0.6%. The reason for slight improvement is that their images are object-centric with simple background. Hence DeepHOT cannot bring its superiority into full play, which can be robust to complex background due to image-level OT that provides meaningful distances when the supports of the distributions do not overlap.

**Results on Digits.** Table 3 lists performance of DeepHOT compared with a series of other state-of-the-art methods. As can be seen, DeepHOT achieves a comparable or higher score to the current state-of-the-art methods. It is considerably important that we see increases of the performance among all scenarios compared with JUMBOT that is the most related to our approach. DeepHOT outperforms the competitors with the exception of CDAN-E that has slightly better performance on U→M with 0.2% margin. The improvement on digits dataset is significant although it enhances not too much, since the accuracy on digits dataset itself is relatively high and is difficult to further improve.

**Results on VisDA.** Table 4 gathers results on VisDA dataset, where our method achieves the best accuracy on the validation set with a margin of 1%. The reported results are convincing since the dataset is large-scale.

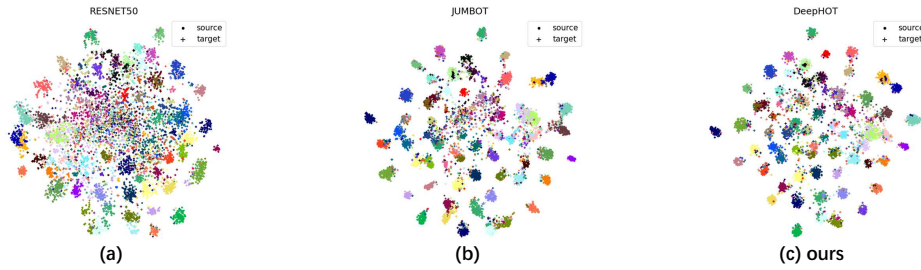


Figure 2: The t-SNE visualization. Representations of task C→P on Office-Home dataset (65 classes) are visualized in (a)-(c), where each color denotes a **class**.

Table 5: Ablation study of DeepHOT for task C→R on Office-Home.

	Domain-level		Image-level			Accuracy
	EMD	UOT	$l_2$	$\mathcal{L}_{ce}$	SWD	
(a)		✓	✓			68.1
(b)	✓		✓	✓		71.4
(c)		✓	✓	✓		74.9
(d) <b>ours</b>		✓	✓	✓	✓	<b>78.0</b>

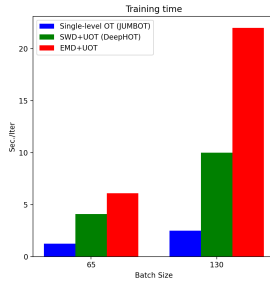


Figure 3: Comparison of training time.

## Ablation Study

In ablation study, we first validate the efficacy of each component in DeepHOT for both domain-level and image-level, and then we compare the training speed among different implementations of OT formulation to prove the efficiency of DeepHOT. More experiments regarding the ablation study and the robustness to batch size and the number of projections are presented in supplementary materials. We follow the setting of hyper-parameters on Office-Home and each experiment in ablation study adopts the same setting.

**Component validation.** As shown in Table 5, for domain-level OT, we observe that UOT leads to a better performance by comparing the experiments (b) EMD (i.e., origin OT formulation) and (c), where the performance gain of UOT achieves 3.5%. For image-level OT, the effectiveness of SWD can be proven from the experiment (c) and (d) in which the performance with SWD further increases 3.1%.

**Training efficiency.** To show the efficiency of SWD on image-level OT, we compare the training time between original OT (a.k.a EMD) and SWD that are combined with

domain-level OT (UOT), as well as single-level OT. This experiment runs on the same *GeForce GTX 1080Ti* with 4 GPUs. We test the training time on task C→R of Office-Home from 10th iteration to 100th iteration and get the averaged results. The number of projections in SWD is fixed at 128. The results are shown in Fig. 3. We see that DeepHOT with SWD+UOT (green) achieves a faster speed than that with EMD+UOT (red), which approaches single-level OT method (blue) much more. It suggests our solution is more efficient among Hierarchical OT-based methods.

## Visualization Analysis

To present the effectiveness of adaptation process more intuitively, the representations of various methods (no-adaptation, JUMBOT and DeepHOT) are visualized by t-SNE (Van der Maaten and Hinton 2008) technique, as shown in Fig. 2. Here we only show the C→P scenario, and more cases are presented in supplementary materials. Obviously, the source and target are not aligned without adaptation process, as presented in Fig. 2(a). Fig. 2(b) shows that domains can be aligned by JUMBOT but categories are not discriminative well. However, as shown in the center of Fig. 2(b) and (c), intuitively the sample points of (b) are more scattered than that of (c), while the boundaries of clusters marked with different colors for different categories in (c) are more clear. This suggests that our proposal is able to enhance category-discriminative representations while aligning domains.

## Conclusion

In this paper, we tackle two important issues for unsupervised domain adaptation. First, how to learn domain-invariant yet category-discriminative representations? We propose the deep hierarchical optimal transport framework, which uses the domain-level OT to learn domain-invariant representations, and adopts the image-level OT to capture category-discriminative features. Second, how to build a robust and efficient DeepHOT model? We exploit unbalanced mini-batch optimal transport and sliced Wasserstein distance in domain-level and image-level OTs, respectively. The effectiveness and efficiency of the proposed DeepHOT method are verified by the extensive experiments on four benchmark datasets. It is worth noting DeepHOT is a generalized framework. We will try different implementations of DeepHOT in the future.



## References

- Balaji, Y.; Chellappa, R.; and Feizi, S. 2020. Robust optimal transport with applications in generative modeling and domain adaptation. *Advances in Neural Information Processing Systems*, 33: 12934–12944.
- Chen, M.; Zhao, S.; Liu, H.; and Cai, D. 2020. Adversarial-learned loss for domain adaptation. In *Proceedings of the AAAI Conference on Artificial Intelligence*, volume 34, 3521–3528.
- Chizat, L.; Peyré, G.; Schmitzer, B.; and Vialard, F.-X. 2018. Scaling algorithms for unbalanced optimal transport problems. *Mathematics of Computation*, 87(314): 2563–2609.
- Courty, N.; Flamary, R.; Habrard, A.; and Rakotomamonjy, A. 2017a. Joint distribution optimal transportation for domain adaptation. *Advances in Neural Information Processing Systems*, 30.
- Courty, N.; Flamary, R.; and Tuia, D. 2014. Domain adaptation with regularized optimal transport. In *Joint European Conference on Machine Learning and Knowledge Discovery in Databases*, 274–289. Springer.
- Courty, N.; Flamary, R.; Tuia, D.; and Rakotomamonjy, A. 2017b. Optimal Transport for Domain Adaptation. *IEEE Transactions on Pattern Analysis and Machine Intelligence*, 39(9): 1853–1865.
- Damodaran, B. B.; Kellenberger, B.; Flamary, R.; Tuia, D.; and Courty, N. 2018. Deepjdot: Deep joint distribution optimal transport for unsupervised domain adaptation. In *Proceedings of the European Conference on Computer Vision (ECCV)*, 447–463.
- Fatras, K.; Séjourné, T.; Flamary, R.; and Courty, N. 2021. Unbalanced minibatch optimal transport; applications to domain adaptation. In *International Conference on Machine Learning*, 3186–3197. PMLR.
- Flamary, R.; and Courty, N. 2017. Pot python optimal transport library. *GitHub*: <https://github.com/rflamary/POT>, 144.
- Frogner, C.; Zhang, C.; Mobahi, H.; Araya, M.; and Poggio, T. A. 2015. Learning with a Wasserstein loss. *Advances in neural information processing systems*, 28.
- Ganin, Y.; Ustinova, E.; Ajakan, H.; Germain, P.; Larochelle, H.; Laviolette, F.; Marchand, M.; and Lempitsky, V. 2016. Domain-adversarial training of neural networks. *The journal of machine learning research*, 17(1): 2096–2030.
- Gretton, A.; Sejdinovic, D.; Strathmann, H.; Balakrishnan, S.; Pontil, M.; Fukumizu, K.; and Sriperumbudur, B. K. 2012. Optimal kernel choice for large-scale two-sample tests. *Advances in neural information processing systems*, 25.
- Hamri, M. E.; Bennani, Y.; Falih, I.; and Ahaggach, H. 2021. Hierarchical Optimal Transport for Unsupervised Domain Adaptation. *arXiv preprint arXiv:2112.02073*.
- He, K.; Zhang, X.; Ren, S.; and Sun, J. 2016. Identity mappings in deep residual networks. In *European conference on computer vision*, 630–645. Springer.
- Huang, J.; Guan, D.; Xiao, A.; Lu, S.; and Shao, L. 2022. Category contrast for unsupervised domain adaptation in visual tasks. *IEEE/CVF Conference on Computer Vision and Pattern Recognition*.
- Hull, J. J. 1994. A database for handwritten text recognition research. *IEEE Transactions on pattern analysis and machine intelligence*, 16(5): 550–554.
- Kantorovich, L. V. 2006. On the translocation of masses. *Journal of mathematical sciences*, 133(4): 1381–1382.
- Le, T.; Nguyen, T.; Ho, N.; Bui, H.; and Phung, D. 2021. Lamda: Label matching deep domain adaptation. In *International Conference on Machine Learning*, 6043–6054. PMLR.
- LeCun, Y.; Bottou, L.; Bengio, Y.; and Haffner, P. 1998. Gradient-based learning applied to document recognition. *Proceedings of the IEEE*, 86(11): 2278–2324.
- Lee, C.-Y.; Batra, T.; Baig, M. H.; and Ulbricht, D. 2019a. Sliced wasserstein discrepancy for unsupervised domain adaptation. In *Proceedings of the IEEE/CVF Conference on Computer Vision and Pattern Recognition*, 10285–10295.
- Lee, J.; Dabagia, M.; Dyer, E.; and Rozell, C. 2019b. Hierarchical optimal transport for multimodal distribution alignment. *Advances in Neural Information Processing Systems*, 32.
- Liero, M.; Mielke, A.; and Savaré, G. 2018. Optimal entropy-transport problems and a new Hellinger–Kantorovich distance between positive measures. *Inventiones mathematicae*, 211(3): 969–1117.
- Liu, M.-Y.; Breuel, T.; and Kautz, J. 2017. Unsupervised image-to-image translation networks. *Advances in neural information processing systems*, 30.
- Long, M.; Cao, Y.; Wang, J.; and Jordan, M. 2015. Learning transferable features with deep adaptation networks. In *International conference on machine learning*, 97–105. PMLR.
- Long, M.; Cao, Z.; Wang, J.; and Jordan, M. I. 2018. Conditional adversarial domain adaptation. *Advances in neural information processing systems*, 31.
- Luo, D.; Xu, H.; and Carin, L. 2020. Hierarchical optimal transport for robust multi-view learning. *arXiv preprint arXiv:2006.03160*.
- Netzer, Y.; Wang, T.; Coates, A.; Bissacco, A.; Wu, B.; and Ng, A. Y. 2011. Reading digits in natural images with unsupervised feature learning. *NIPS Workshop on Deep Learning and Unsupervised Feature Learning*.
- Nguyen, T.; Le, T.; Zhao, H.; Tran, H. Q.; Nguyen, T.; and Phung, D. 2021. Tidot: A teacher imitation learning approach for domain adaptation with optimal transport. *IJCAI*.
- Peng, X.; Usman, B.; Kaushik, N.; Hoffman, J.; Wang, D.; and Saenko, K. 2017. Visda: The visual domain adaptation challenge. *arXiv preprint arXiv:1710.06924*.
- Redko, I.; Habrard, A.; and Sebban, M. 2017. Theoretical analysis of domain adaptation with optimal transport. In *Joint European Conference on Machine Learning and Knowledge Discovery in Databases*, 737–753. Springer.
- Saenko, K.; Kulis, B.; Fritz, M.; and Darrell, T. 2010. Adapting visual category models to new domains. In *European conference on computer vision*, 213–226. Springer.
- Sankaranarayanan, S.; Balaji, Y.; Castillo, C. D.; and Chellappa, R. 2018. Generate to adapt: Aligning domains using generative adversarial networks. In *Proceedings of the IEEE*



*conference on computer vision and pattern recognition*, 8503–8512.

Shmelkov, K.; Schmid, C.; and Alahari, K. 2017. Incremental learning of object detectors without catastrophic forgetting. In *Proceedings of the IEEE international conference on computer vision*, 3400–3409.

Sun, B.; and Saenko, K. 2016. Deep coral: Correlation alignment for deep domain adaptation. In *European conference on computer vision*, 443–450. Springer.

Sutskever, I.; Martens, J.; Dahl, G.; and Hinton, G. 2013. On the importance of initialization and momentum in deep learning. In *International conference on machine learning*, 1139–1147. PMLR.

Taherkhani, F.; Dabouei, A.; Soleymani, S.; Dawson, J.; and Nasrabadi, N. M. 2020. Transporting labels via hierarchical optimal transport for semi-supervised learning. In *European Conference on Computer Vision*, 509–526. Springer.

Tzeng, E.; Hoffman, J.; Saenko, K.; and Darrell, T. 2017. Adversarial discriminative domain adaptation. In *Proceedings of the IEEE conference on computer vision and pattern recognition*, 7167–7176.

Tzeng, E.; Hoffman, J.; Zhang, N.; Saenko, K.; and Darrell, T. 2014. Deep domain confusion: Maximizing for domain invariance. *arXiv preprint arXiv:1412.3474*.

Van der Maaten, L.; and Hinton, G. 2008. Visualizing data using t-SNE. *Journal of machine learning research*, 9(11).

Venkateswara, H.; Eusebio, J.; Chakraborty, S.; and Panchanathan, S. 2017. Deep hashing network for unsupervised domain adaptation. In *Proceedings of the IEEE conference on computer vision and pattern recognition*, 5018–5027.

Wang, J.; Chen, Y.; Feng, W.; Yu, H.; Huang, M.; and Yang, Q. 2020. Transfer learning with dynamic distribution adaptation. *ACM Transactions on Intelligent Systems and Technology (TIST)*, 11(1): 1–25.

Xiao, N.; and Zhang, L. 2021. Dynamic weighted learning for unsupervised domain adaptation. In *Proceedings of the IEEE/CVF Conference on Computer Vision and Pattern Recognition*, 15242–15251.

Yan, H.; Ding, Y.; Li, P.; Wang, Q.; Xu, Y.; and Zuo, W. 2017. Mind the class weight bias: Weighted maximum mean discrepancy for unsupervised domain adaptation. In *Proceedings of the IEEE conference on computer vision and pattern recognition*, 2272–2281.

Yurochkin, M.; Clatici, S.; Chien, E.; Mirzazadeh, F.; and Solomon, J. M. 2019. Hierarchical optimal transport for document representation. *Advances in Neural Information Processing Systems*, 32.

Zhang, C.; Cai, Y.; Lin, G.; and Shen, C. 2020. Deepemd: Few-shot image classification with differentiable earth mover’s distance and structured classifiers. In *Proceedings of the IEEE/CVF conference on computer vision and pattern recognition*, 12203–12213.

Zhang, X.; Yu, F. X.; Chang, S.-F.; and Wang, S. 2015. Deep transfer network: Unsupervised domain adaptation. *arXiv preprint arXiv:1503.00591*.